Journal of Materials Chemistry

Cite this: J. Mater. Chem., 2012, 22, 3549

www.rsc.org/materials

PAPER

Coaxial multi-shelled TiO_2 nanotube arrays for dye sensitized solar cells†

Jijun Qiu,[a] Fuwei Zhuge,[a] Xiaomin Li,*[a] Xiangdong Gao,[a] Xiaoyan Gan,[a] Lin Li,[b] Binbin Weng,[b] Zhisheng Shi*[b] and Yoon-Hwae Hwang[c]

Received 20th October 2011, Accepted 7th December 2011
DOI: 10.1039/c2jm15354h

The performance of one-dimensional (1D) TiO_2 nanotube based dye-sensitized solar cells (DSCs) was limited by the insufficient surface area of TiO_2 nanotubes. To solve this issue, coaxial multiple-shelled TiO_2 nanotube arrays were successfully synthesized on the transparent conductive oxide (TCO) substrates by using improved ZnO nanorod template assisted layer by layer absorption and reaction (LbL-AR) technique. To fabricate tube-in-tube nanostructures, LbL-AR TiO_2 coatings were successively deposited on the exterior walls of the ZnO nanowires and the sacrificial sol–gel ZnO spacers, which were removed together by selective etching to form the hollow tubal structures. The performance of dye-sensitized solar cells (DSCs) increases with increasing the shell number of multi-shelled TiO_2 nanotube photoanodes, attributed to the increase of the surface area, which was confirmed by N_2 adsorption-desorption isotherms and the dye-loading capacities. A maximum efficiency of 6.2% was achieved for a quintuple shelled TiO_2 nanotube photoanode with a short-circuit current density (J_{sc}) = 15 mA cm^2, open-circuit voltage (V_{oc}) = 0.73 V and fill factor (FF) = 0.57.

1 Introduction

As next-generation solar-to-electric energy conversion devices, dye-sensitized solar cells (DSCs) are of great interest as a cost-effective alternative to conventional silicon photovoltaic devices.[1] The highest efficiency of exceeding 12.3% has already been achieved in porous TiO_2 nanocrystalline DSCs,[2] however, it is still lower than that of silicon photovoltaic devices. The lower efficiency is primarily a consequence of electron recombination during the charge transport processes, resulting from the presence of tremendous crystalline boundaries and disordered pore structures. To solve this issue, considerable efforts have been devoted to one-dimensional (1D) structures, such as nanorod (NRs) and nanotubes (NTs), persuing the profits on internal light trapping effect, fast electron transport and fluent redox penetration. However, the 9% maximum efficiency of TiO_2 NTs DSCs is still below the efficiency of TiO_2 nanocrystalline DSCs,[3] which is primarily ascribed to the insufficient surface area (dye-loading capacity) of simple 1D TiO_2 NTs. Therefore, considerable efforts have been paid to the secondary structural design of TiO_2 NTs,[4] including modifying the tube walls with mesopores,[4a,4b] decorating with quantum dots[4c] or nanoparticles[4d] and creating defined bamboo-type rings.[4e]

Recently, double-shelled TiO_2 nanotube arrays (NTAs) have attracted lots of attention for their superior specific surface area, abundant and tunable multi-level interior structures, flexible chemical composition and multiphase anisotropic interfaces.[5] In this respect, several synthesis methods come into being, including self-organization,[5a] electrochemical-anodization,[5b,5c] high-temperature treatment[5d] and template-directed synthesis.[5e] However, owing to a structural complexity, it is still an unsolved technological challenge to generate multi-shelled TiO_2 NTAs with a precise structural controllability on the transparent conductive substrates (TCO) by using a simple and low-cost route, which restricts its large-scale production and application in DSCs.

Based on our previous works in fabrication of simple single-shelled TiO_2 NTAs,[4b,6] herein, a ZnO NR template-directed procedure is proposed to fabricate multi-shelled TiO_2 NTAs on TCO substrates. At the same time, we studied the shell number of multi-shelled TiO_2 NTAs dependence of the surface area (dye-loading capacity). Additionally, the effects of TiO_2 NTAs on the performance and electron transport properties of DSCs were investigated by using electrochemical impedance spectra (EIS), showing a similar electrical properties with anodized TiO_2 nanotubes.

[a]State Key Laboratory of High Performance Ceramics and Superfine Microstructures, Shanghai Institute of Ceramics, Chinese Academy of Sciences, Shanghai, 200050, China. E-mail: lixm@mail.sic.ac.cn; Fax: +86-021-52413122; Tel: +86-021-52412554
[b]School of Electrical and Computer Engineering, University of Oklahoma, Norman, Oklahoma, 73019, USA. E-mail: lixm@mail.sic.ac.cn; Fax: +1-405-525-7066; Tel: +1-405-525-4292
[c]Department of Nano-Materials Engineering & BK 21 Nano Fusion Technology Division, Pusan National University, Miryang, 627-706, Korea

† Electronic supplementary information (ESI) available: Fig. S1-S6 show: schematic fabrication procedure of LbL-AR for TiO_2 shells; high-magnification FESEM images of ZnO spacing layer and multi-shelled TiO_2 NTs; FESEM and TEM images of multi-shelled TiO_2 NTAs with different shell numbers; high-magnification top-view FESEM images of broken tips of multi-shelled TiO_2 NTs with different shell numbers; characteristics of high-density triple-shelled TiO_2 NTAs; and model circuit of the multi-shelled TiO_2 NTAs DSSCs. See DOI: 10.1039/c2jm15354h

2 Experimental

2.1 Fabrication and characterizations of multi-shelled TiO_2 NTAs

2.1.1 ZnO-doped TiO_2 seed layer on F-doped SnO_2 (FTO) substrate by using a sol–gel method. ZnO doped TiO_2 seed layers were deposited on FTO substrates by using the sol–gel method to induce the vertical growth of ZnO NRAs template, and to enhance the adhesion between the multi-shelled TiO_2 NTAs and substrate after removing ZnO NRAs templates. Firstly, 0.5 M titanium butoxide and 0.5 M acetylacetone were dissolved in ethanol solution at room temperature and vigorously stirred for 2 h to yield a homogeneous pure TiO_2 sol. Then, 0.05 M zinc acetate dehydrate was introduced into the TiO_2 sol and continuously stirred for 2 h to obtain ZnO doped TiO_2 sol. The cleaned FTO substrates (50 × 25 mm) were dipped into the ZnO doped TiO_2 sol, withdrawn at 3.0 mm s^{-1} and then heated to 550 °C at 5 °C min^{-1} for 1 h to obtain dense and transparent ZnO doped TiO_2 seed layers on the FTO substrates.

2.1.2 Aligned ZnO NRAs template by using a hydrothermal method. The hydrothermal solution for aligned ZnO NRAs templates was prepared by dissolving zinc nitrate hexahydrate, hexamethylenetetramine and polyethylenimine (branched, low molecular weight) in distilled water with a concentration ratio of 0.02 : 0.02 : 0.0005. 150 ml solution was first sealed in a glass bottle of maximum volume 250 ml and was then heated to 95 °C for 0.5 h. Then the ZnO doped TiO_2-seeded FTO substrates were quickly immersed in the hot solution and tilted against the wall of the bottle with the seed layers facing down. Subsequently the bottle was heated to 95 °C for 12 h without any stirring. The hot solution was refreshed every 12 h for a sufficient growth rate of 0.4∼0.5 μm h^{-1} till the desired lengths were achieved.[6d]

2.1.3 Assembly of TiO_2 shell by using layer-by-layer absorption and reaction (LbL-AR) method. Multi TiO_2 shells were assembled over ZnO NRTAs templates by using LbL-AR coating technique, which was carried in a homemade three-dimensional autonomic dip-coating apparatus. As shown in Fig. S1† of supporting information, one LbL-AR cycle involves four successive steps: (1) to adsorb titanium species by immersing ZnO NRAs templates into the TiO_2 sol (as above); (2) to remove loosely bounded titanium species by rinsing in ethanol; (3) to form TiO_2 coating by immersing into distilled water, and (4) to remove weak-bounded TiO_2 nanoparticles by rinsing in ethanol. A cycle thickness is about 0.8 nm with a 30 s immersion time, and the TiO_2 shell thicknesses were tailored by adjusting the LbL-AR cycle number. Then, the ZnO/TiO_2 core/shell samples were calcined at 300 °C for 1 h to remove the organic residuals.[6a]

2.1.4 Deposition of sacrificial ZnO spacers by sol–gel method. The sacrificial ZnO spacers were deposited over TiO_2 shell by dip-coating ZnO sol, prepared by dissolving 0.75 M zinc acetate dehydrate and 0.75 M monoethanolamine in 2-methoxyethanol solution. TiO_2 shell coated ZnO NRAs templates were dipped into ZnO sol, withdrawn at 2.0 cm min^{-1} and preheated at 300 °C for 5 min. The above cycle was repeated until the desired spacer thickness was achieved with a 1.5 nm deposition rate.

In order to obtain multiple layered TiO_2 shell/ZnO spacer structures, the assemblies of TiO_2-LbL-AR and ZnO-SG were alternately carried out.

2.1.5 Removing ZnO NRAs template and ZnO spacers by wet-chemical etching method. To obtain tube in tube nanostructures, the ZnO NRAs templates and ZnO spacers were removed by a selective wet chemical etching in dilute aqueous solution of $TiCl_4$ (0.015 M) at room temperature. Here, the etching time various from 1.5 to 3 h, depending on the shell number of multi-shelled TiO_2 NTAs. The etched multi-shelled TiO_2 NTAs were then calcined at 550 °C for 1 h for crystallization.

2.1.6 Characterizations of multi-shelled TiO_2 NTAs. The multi-shelled nanotubal structures were observed by a field-emission scanning electron microscopy (FESEM, Hitachi S-4700) and a transmission electron microscopy (TEM, JEOL JEM-2100F). BET surface areas and pore size distributions were characterized by using a micrometerics ASP2000 surface area analyzer. Dye desorption experiments in dilute NaOH solution were also conducted to verify the surface area information, assuming monolayer dye molecular coverage on TiO_2 surface.

2.2 Fabrication and photovoltaic characterizations of multi-shelled TiO_2 NTAs DSCs

Before being assembled into DSCs, the multi-shelled TiO_2 NTAs were all sculptured to a fixed squire shape of 0.42 cm^2 and immersed into 70 °C $TiCl_4$ solution (0.04 M) for 1 h for post treatment, followed by a heat-treatment at 500 °C for 1 h. Subsequently, the multi-shelled TiO_2 NTAs were sensitized in N719 (0.0005 M) ethanol solution for 12 h. The catalytic counter electrodes are 50 nm thick Pt coated FTO glass, deposited by an e-beam evaporation. Hot-melt polypropylene spacers with a thickness of 100 μm were used to seal the photoanodes and counter electrodes into sandwich cells. The electrolyte (0.5 M tetrabutylammonium iodide, 0.05 M I_2 and 0.5 M 4-tertbutylpyridine in acetonitrile), was then introduced by injection and capillary force. Silver contacts were made on the electrodes by colloidal silver paste to minimize the contact resistance during the photovoltaic measurements. An aperture mask with the same area of 0.25 cm^2 as the photoanode was employed during the characterization for the calibration of the cell area.

Photovoltaic characterizations of fabricated Multi-shelled DSCs were conducted on an electrochemical workstation (CHI-660B), simulated AM1.5 illumination (100 mW cm^{-2}) is provided by an Oriel simulator (300 W, 91160B). *J–V* curves were measured by sweeping the bias voltage in the range from 0 to 0.85 V, and electrochemical impedance spectra (EIS) were measured at open circuit voltage with an ac bias signal of 10 mV in the frequency range from 10^{-1} to 10^5 Hz. The OCVD was conducted by switching off the illumination of the solar simulator in a dark environment.

3 Results and discussion

The overall strategy is illustrated in Scheme 1, involving a fabrication of ZnO NR template by a hydrothermal method, an

assembly of TiO_2 shells by LbL-AR, a deposition of ZnO sacrificial spacer layers by a sol–gel dip-coating technique, and a removing of ZnO NR templates and space layers by a selective wet-chemical etching route. It is reasonable to employ hydrothermal synthesized ZnO NRs as positive template to fabricate simple NTs[6,7] and complex NTAs, in consideration of its low-temperature, structural versatility, facile large-scale production and fast etching rate. Besides, the structural characteristics of ZnO NR templates could be custom tailored by adjusting the hydrothermal growth process, providing a versatile route to modulate the structural features of the resultant TiO_2 NTs, including length, inner-diameter and population density. Coaxial multi-layered core-shell nanostructures are constructed by alternately assembling conformal TiO_2 shells and ZnO spacer layers on the surface of ZnO NR templates by LbL-AR and sol–gel methods, respectively. Compared with other backfilling approaches, such as atomic layer deposition (ALD),[8] LbL-AR and sol–gel methods are distinguished from others by their low-cost, good shaping ability and flexible structural controllability.[6,9] Importantly, the nano-scale thicknesses of TiO_2 shells and ZnO spacer layers can be precisely tailored by the surface absorbed precursors, which are further related with corresponding precursor concentration and dip-coating cycle number. In addition to being etching solution to remove ZnO NR templates and ZnO space layers for the hollow coaxial nanotubal structures, diluted $TiCl_4$ solution is well-selected to further increase the surface area by attaching small TiO_2 clusters formed from the hydrolysis of $TiCl_4$ on the surface of original NTs.[6b] Moreover, for maintaining high alignment and good adhesion even after suffering from a long-time etching, which is necessary to completely remove ZnO NR templates, 10% (mol ratio) ZnO doped TiO_2 thin films with high-acid stability, instead of conventional ZnO seed layers, are pre-deposited over FTO substrates to induce the orientated growth of ZnO NR templates and to prevent the multi-shelled TiO_2 NTAs peeling off from FTO substrates due to deep acid-etching.

By now, aligned multi-shelled TiO_2 NTAs from double to sextuple shells have been successfully fabricated by using ZnO NR templates directed method. Fig. 1a–f show a series of TEM images of multi-shelled TiO_2 NTs with various shell numbers from single to sextuple, demonstrating the technical feasibility for coaxial multi-shelled NTs. The inner-diameter of multi-shelled TiO_2 NTAs is consistent with the diameter of ZnO NR templates, indicating a good shaping ability of LbL-AR. Every individual TiO_2 shell is clearly discernible, showing a uniform thickness along the length of nanotube. Noticeably, the TiO_2 shell becomes rougher with increasing the shell number, which is due to the accumulation on the rough surface of sol–gel ZnO space layers, originating from its crystalline nature, as shown in Fig. S2†. High-magnification TEM image and selected-area electron diffraction (SAED) pattern, as shown in Fig. 1g, h, demonstrate that the TiO_2 shell is constructed by stacking anatase nanocrystallines with a diameter of 3–5 nm. The energy dispersive spectroscopy (EDS) pattern in Fig. 1i reveals O and Ti peaks, indicating ZnO NRs were completely removed. The typical side-view FESEM image of the multi-shelled TiO_2 NTAs grown on the FTO substrates, Fig. 1j, shows that the TiO_2 NATs possess closed tips and remain the aligned orientation perpendicular to TCO substrate surface after removing ZnO NR templates, indicating a good adhesion between multi-shelled TiO_2 NTAs and the substrates. The coaxial tube-in-tube structures can be obviously observed from the high magnification top-FESEM image captured from broken edges, as shown in Fig. 1k. More structural characterizations of the multi-shelled TiO_2 NTAs with various shell numbers are exhibited in Fig. S3 and S4†.

The structural parameters of multi-shelled TiO_2 NTAs, including the inner-diameter, length, density, TiO_2 shell thickness, inter-shell spacing, shell number and population density, also can be modulated over a wide range, indicating an excellent structural controllability and flexibility for ZnO NR templates directed LbL-AR process. The inner-diameter, length and population density of multi-shelled TiO_2 NTAs, which are

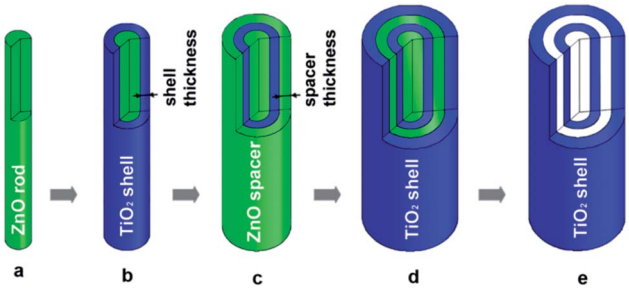

Scheme 1 Schematic illustration of synthetic process for coaxial double-shelled TiO_2 NTAs. (a) ZnO NR template obtained from hydrothermal method, (b) the 1st TiO_2 shell coated by LbL-AR method, (c) the 1st ZnO spacer deposited by sol–gel method, (d) the 2nd TiO_2 shell coated again by LbL-AR, and (e) double-shelled TiO_2 NTAs after etching ZnO NR template and spacers. Multi-shelled TiO_2 NTAs with shell number more than double can be obtained by repeating step (c) and step (d).

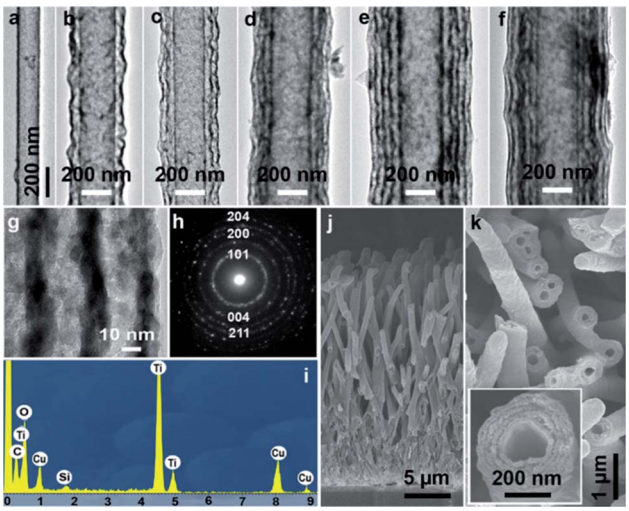

Fig. 1 Characteristics of multi-shelled TiO_2 NTAs with various shell numbers. Low-magnification TEM images of (a) single-, (b) double-, (c) triple-, (d) quadruple-, (e) quintuple- and (f) sextuple-shelled TiO_2 NT. (g) Typical high-magnification TEM image and (h) its corresponding SEAD pattern and (i) EDS result of a triple-shelled TiO_2 NT. Typical low-magnification (j) side-view and (k) top-view FESEM images of a quintuple shelled TiO_2 NTAs grown on the TCO substrate. A high-magnification FESEM image of a broken tip of a quintuple-shelled TiO_2 NT is shown in inset, Fig. 1k.

dependent upon that of ZnO NR templates, could be tuned in the range from 60 to 500 nm, from 5 to 100 μm and from 10^6 to 10^{10} cm^{-2} by tailoring zinc precursor concentration, growth time and doped ZnO content in TiO_2 seed layer, respectively.[6b,6d] By optimizing precursor sol concentrations and drying-times, desired deposition rates of 0.5 nm and 1.5 nm could be achieved for TiO_2 shells and ZnO space layers, respectively. Therefore, the TiO_2 shell thickness and inter-shell spacing could be precisely tailored from 7 to 20 nm and from 8 to 50 nm by controlling the dip-coating cycle number of TiO_2 LbL-AR and ZnO sol–gel, as demonstrated in Fig. 2.

Theoretically, the shell number is dominated by the TiO_2 shell thickness, the inter-shell spacing and distance between adjacent ZnO nanorods. The nano-scale thicknesses controllability in TiO_2 shells and inter-shell spacing makes it possible to continuously increase the shell number. Therefore, the maximum shell number is only limited by the initial distance between adjacent ZnO NRs, which is related with its population density, as shown in Fig. S5† . Noticeably, the shell number could be further increased after extending the initial distance between adjacent ZnO NRs with a sacrifice of population density. However, it is possible to result in a decrease of total surface area.

The porous characterization of multi-shelled TiO_2 NTAs was investigated by the N_2 adsorption-desorption isotherms. As shown in Fig. 3a, all N_2 adsorption-desorption isotherms of multi-shelled TiO_2 NTAs with various shell number possess typical IV curves with H_1 hysteresis loops, indicating the co-presence of mesopores and macropores.[4a] Based on the FESEM and TEM images, the opening mesoporous structure, which is characterized at pressure of 0.45–0.8 , derives from the non-close-packed structure of TiO_2 nanocrystalline shells, and the macroporous structures at relative high pressure of 0.9∼1.0 is ascribed to the large inner channels of the TiO_2 NTs. The Barrett–Joyner–Halenda (BJH) pore diameter distribution plot shows that a narrow size distribution centered from 2.9 to 3.2 nm, as shown in Fig. 3b. The Brunauer–Emmett–Teller (BET) specific surface area, summarized in Fig. 3c, dramatically increases from 119

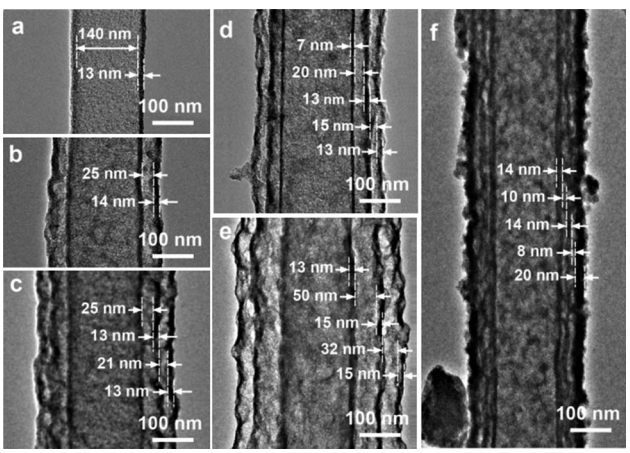

Fig. 2 Typical TEM images of triple-shelled TiO_2 NTs with different structural features. (a) Single-, (b) double- and (c) triple-shelled TiO_2 NTs with the same shell thickness and intershell distance. Triple-shelled TiO_2 NT with (d) a narrow (d) a wider intershell distance and (f) a thick outer shell.

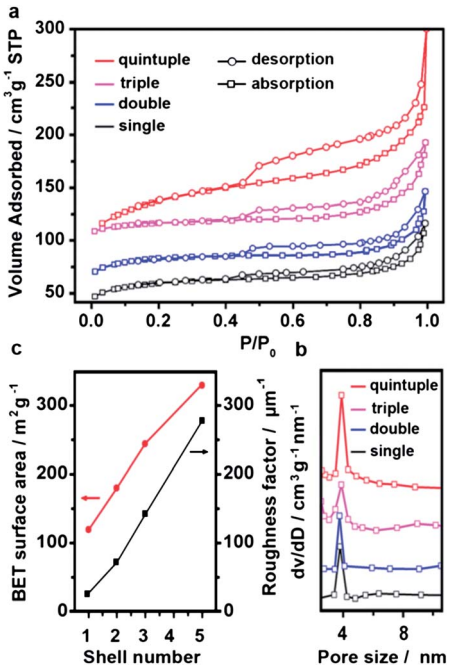

Fig. 3 N_2 adsorption-desorption measurements of the multi-shelled TiO_2 NTs with different shell numbers. (a) N_2 adsorption-desorption isotherm plots, (b) pore size distribution curve and (c) plot of the BET and RF of multi-shelled TiO_2 NTAs *versus* the shell number.

to 331 m^2 g^{-1} with increasing the shell number from single to quintuple, which is higher than that of nanoparticles (∼80 m^2 g^{-1})[10a] and dense nanotube arrays obtained from Ti anodization (∼30 m^2 g^{-1}).[10b] The continuous increase in the BET is attributed to the shell being more and more coarse with raising the shell number, which is confirmed by the series of TEM images (Fig. 1a–f, Fig. 2) and FESEM images (Fig. S2, S3, S4†). The surface area enhancement is described by the surface roughness factor (RF), defined as the total surface area per volume of NTAs, can be calculated by the form: $RF = BET \times m/L$, where m is mass per unit substrate area (g m^{-2}), L is the thickness of multi-shelled TiO_2 NTAs (μm). As shown in Fig. 3c, there is a linear relationship between the shell number and the RF, and RF of the triple-shelled TiO_2 NTAs exceeds 100 μm^{-1} of porous nanocrystalline TiO_2 films,[10] being necessary for good light harvesting with ruthenium based sensitizers.

Prior to dye adsorption, the multi-shelled TiO_2 NTAs were hydrothermal treated in $TiCl_4$ aqueous solution at 70 °C to improve bonding between the TiO_2 and the dye for a better charge injection.[11] The dye-loading capacities of multi-shelled TiO_2 NTAs, examined by desorbing the dye molecular in dilute NaOH solution and measuring the absorption spectra, are collected in Table 1. For 25 μm-thick multi-shelled TiO_2 NTAs, as expected, the increase in shell number from single to quintuple leads to a significantly enhanced dye-loading capacity from 2.16×10^{-8} to 9.17×10^{-8} mol cm^{-2}. However, the dye-loading capability is not proportional to the corresponding RF (or surface area), suggesting that not all surfaces of TiO_2 pores shells have been completely sensitized.

Fig. 4a shows the current–voltage characteristics of N719-DSCs fabricated by using multi-shelled TiO_2 NTAs with various

Table 1 Photovoltaic parameters of the DSCs made of the multi-shelled TiO_2 NTAs with various shell numbers

Shell number	V_{oc} (V)	J_{sc} (mA cm^{-2})	FF (%)	η (%)	D (mol cm^{-2})	R_w (Ω)	R_k (Ω)	C_p (mF)	τ_r (s)
1	0.79	6.59	64.3	3.35	2.16	0.32	32.6	1.32	0.16
2	0.76	9.08	63.7	4.40	3.82	0.55	21.8	1.87	0.16
3	0.73	12.1	57.1	5.15	5.34	0.63	10.8	3.82	0.16
5	0.73	15.0	56.6	6.20	9.07	0.72	8.04	5.28	0.16

shell numbers, and the detailed parameters are summarized in Table 1. As shown in Table 1, despite of a decrease in the open circuit voltage (V_{oc}) from 0.79 to 0.73V and the Fill Factor (FF) from 64.3 to 56.6%, the DSCs photoelectric conversion efficiency (η), which is determined by $\eta \propto J_{sc} \times V_{oc} \times FF$, is significantly improved with increasing the shell number, and a maximum η of 6.20% is achieved with quintuple-shelled TiO_2 NTAs. Therefore, the improvement of DSCs performance is caused by the increment of short circuit current density (J_{sc}) from 6.59 to 15.0 mA cm^{-2}, which certainly originates from the enhanced dye-loading capability due to the increased surface area with shell number. The drop in V_{oc} and FF is a result of increasing the number of the recombination centers accompanied by the magnified surface area, which is further confirmed by electrochemical impedance spectroscopy (EIS) and the open circuit voltage decay (OCVD), as shown in Fig. 4b and 4c, respectively.

EIS was employed to investigate the recombination characteristic across the interface of TiO_2/dye/electrolyte, and the Nyquist plots were fitted by utilizing Zview equivalent circuit modeling software with a built-in extended element (DX type 11-Bisquert #2) based on a diffusion–recombination equivalent circuit,[12] as shown in Fig. S6†. The electron transport properties are summarized in Table 1. The chemical capacitance (C_p), reflecting the surface area variation, clearly shows an enhancement from 1.32 to 5.28 mF, which is consistent with the increase of the dye loading capacity, confirming that the improvement of DSCs performance is due to the increased dye loading capacity with increasing the shell number. However, the electron transport resistance (R_w) slightly increases from 0.32 to 0.72 Ω and the charge-transfer resistance related to recombination of electron (R_k) reduces from 32.6 to 8.04 Ω, which are the origins of the drop in V_{oc} and FF with increasing the shell number. The intrinsic electron lifetime (τ) at V_{oc} is almost the same 0.16 s for all multi-shelled TiO_2 NTAs, indicating an undisturbed recombination dynamics with increasing shell number and the RF. The recombination kinetics was examined by measuring OCVD, and the voltage-dependant electron lifetime is shown in Fig. 4c, which is determined by $\tau = k_B T/e\,(dV_{oc}/dt)^{-1}$, where k_B, T, e and t is the Boltzmann constant, the absolute temperature, the electron charge and the transient time, respectively. No obvious features of surface state facilitated recombination are observed in the low V_{oc} region,[12c] being in accordance with the results derived from EIS.

Although being comparable with performances of the prevailing anodized TiO_2 NTAs DSCs, the efficiency of multi-shelled TiO_2 NTs based DSCs is still lower than that of the nancrystalline DSCs, which is not difficult to attain over 7%. Predictably, however, the performance of multi-shelled TiO_2 NTAs DSCs will be dramatically increased *via* two routes as following: (1) to further increase the specific surface area by depositing TiO_2 shells on the hollow channels of TiO_2 NTAs for a high space utilization rate, which could be achieved by using single-shelled TiO_2 NTAs with open-ended tips as templates; (2) to improve the dye absorption process for a full dye-sensitization of multiple shells.

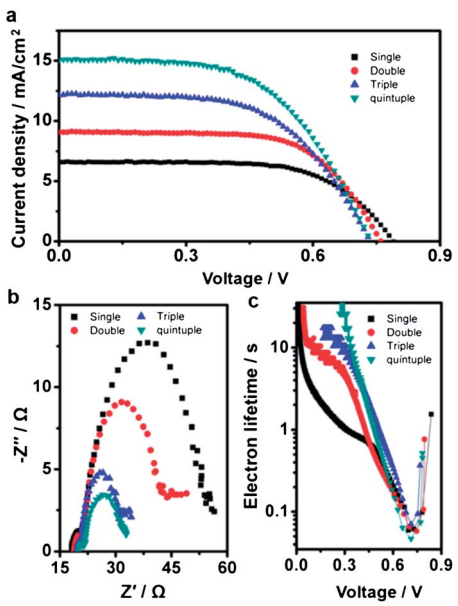

Fig. 4 Photovoltaic characterizations of DSCs as a function of shell number of multi-shelled TiO_2 NTAs photonodes. (a) J–V curves, (b) Nyquist plots and (c) the electron lifetime.

4 Conclusions

In summary, we proposed a very facile and effective wet-chemical scheme, named ZnO NR templates directed LbL-AR assembling approach, to fabricate tube-in-tube nanostructures for efficient DSCs, and coaxial multi-shelled TiO_2 NTAs with double to sextuple shells were successfully fabricated on TCO substrates. The uniform shell thickness and inter-shell spacing can be precisely tuned in nanometre scale just by controlling dip-coating cycle number, indicating a technical feasibility and structural controllability of the synthetic strategy. The specific surface areas and RF of multi-shelled TiO_2 NTAs increase with increasing the shell number, enhancing the dye-loading capacity, therefore, a maximum conversion efficiency of 6.20% has been achieved as using quintuple-shelled TiO_2 NTAs as electrodes in DSCs. Additionally, the scheme can be further expanded to build multi-shelled nanostructures with different materials and geometries, opening a possibility for complex nano-architecture synthesis and engineering in a broad range of nano-technological applications.

Acknowledgements

This work was financially supported by the National Natural Science Foundation of China (51102261, 51002174 and 90922026) and State Key Development Program for Basic Research of China (2009CB623304).

References

1 B. O'Regan and M. Grätzel, *Nature*, 1991, **353**, 737.
2 (*a*) T. Daeneke, T. Kwon, A. B. Holmes, N. W. Duffy, U. Bach and L. Spiccia, *Nat. Chem.*, 2011, **3**, 211; (*b*) A. Yella, H. Lee, H. N. Tsao, C. Yi, A. K. Chandiran, M. K. Nazeeruddin, E. W. Diau, C. Yeh, S. M. Zakeeruddin and M. Grätzel, *Science*, 2011, **334**, 629.
3 B. Lei, J. Liao, R. Zhang, J. Wang, C. Su and D. Kuang, *J. Phys. Chem. C*, 2010, **114**, 15228.
4 (*a*) K. Wang, M. Wei, M. A. Morris, H. Zhou and J. D. Holmes, *Adv. Mater.*, 2007, **19**, 3016; (*b*) J. Qiu, W. Yu, X. Gao and X. Li, *Nanotechnology*, 2007, **18**, 295604; (*c*) H. J. Lee, M. K. Wang, P. Chen, D. P. Gamelin, S. M. Zakeeruddin, M. Grätzel and M. K. Nazeeruddin, *Nano Lett.*, 2009, **9**, 4221; (*d*) P. Roy, D. Kim, I. Paramasivam and P. Schmuki, *Electrochem. Commun.*, 2009, **11**, 1001; (*e*) S. P. Albu, D. Kim and P. Schmuki, *Angew. Chem., Int. Ed.*, 2008, **47**, 1916.
5 (*a*) J. H. Jung, T. Shimizu and S. Shinkai, *J. Mater. Chem.*, 2005, **15**, 3979; (*b*) S. E. John, S. K. Mohapatra and M. Misra, *Langmuir*, 2009, **25**, 8240; (*c*) W. Zhang, Z. Xi, G. Li, Q. Wang, H. Tang, Y. Liu, Y. Zhao and L. Jiang, *Small*, 2009, **5**, 1742; (*d*) S. P. Albu, A. Ghicov, S. Aldabergenova, P. Drechsel, D. LeClere, G. E. Thompson, J. M. Macak and P. Schmuki, *Adv. Mater.*, 2008, **20**, 4135; (*e*) C. Bae, Y. Yoon, H. Yoo, D. Han, J. Cho, B. H. Lee, M. M. Sung, M. G. Lee, J. Kim and H. Shin, *Chem. Mater.*, 2009, **21**, 2574.
6 (*a*) J. Qiu, W. Yu, X. Gao and X. Li, *Nanotechnology*, 2006, **17**, 4695; (*b*) J. Qiu, F. Zhuge, K. Lou, X. Gao, X. Gan, W. Yu and X. Li, *J. Mater. Chem.*, 2011, **21**, 5602; (*c*) F. Zhuge, J. Qiu, X. Li, X. Gao, X. Gan and W. Yu, *Adv. Mater.*, 2011, **223**, 1330; (*d*) J. Qiu, F. Zhuge, X. Gao, X. Gan, W. Yu, X. Li, W. He, S. Park, H. Kim and Y. Hwang, *Nanotechnology*, 2010, **21**, 159602.
7 (*a*) J. Hwang, B. Min, J. S. Lee, K. Keem, K. Cho, M. Y. Sun, M. S. Lee and S. Kim, *Adv. Mater.* **16**, p. 422; (*b*) J. H. Lee, I. C. Leu, M. C. Hsu, Y. W. Chung and M.-H. Hon, *J. Phys. Chem. B*, 2005, **109**, 13056; (*c*) C. Xu, P. H. Shin, L. Cao, J. Wu and D. Gao, *Chem. Mater.*, 2010, **22**, 143; (*d*) J. Goldberger, R. He, S. Lee, Y. Zhang, H. Yan, H. Choi and P. Yang, *Nature*, 2003, **422**, 599; (*e*) J. Xu, C. Y. Luan, Y. B. Tang, X. Chen, J. A. Zapien, W. J. Zhang, H. L. Kwong, X. M. Meng, S. T. Lee and C. S. Lee, *ACS Nano*, 2010, **4**(10), 6064; (*f*) M. Zhou, H. Zhu, X. Wang, Y. Xu, Y. Tao, S. Hark, X. Xiao and Q. Li, *Chem. Mater.*, 2010, **22**, 64.
8 (*a*) D. Gu, H. Baumgart, T. M. Abdel-Fattah and G. Namkoong, *ACS Nano*, 2010, **4**, 753; (*b*) S. W. Choi, J. Y. Park, C. Lee, J. G. Lee and S. S. Kim, *J. Am. Ceram. Soc.*, 2011, **94**, 1974.
9 R. B. Foong, Y. Shen, X. Hu and A. Sellinger, *Adv. Funct. Mater.*, 2010, **20**, 1390.
10 (*a*) J. R. Jennings, A. Ghicov, L. M. Peter, P. Schmuki and A. B. Walker, *J. Am. Chem. Soc.*, 2008, **130**, 13364; (*b*) A. Ghicov, S. Albu, R. Hahn, D. Kim, T. Stergiopoulos, J. Kunze, C. A. Schiller, P. Falaras and P. Schmuki, *Chem.-Asian J.*, 2009, **4**, 520.
11 B. O'Regan, J. R. Durrant, P. M. Sommeling and N. J. Bakker, *J. Phys. Chem. C*, 2007, **111**, 14001.
12 (*a*) M. Adachi, M. Sakamoto, J. Jiu, Y. Ogata and S. Isoda, *J. Phys. Chem. B*, 2006, **110**, 25174; (*b*) J. Bisquer, *J. Phys. Chem. B*, 2002, **106**, 325; (*c*) J. Bisquert, *J. Phys. Chem. C*, 2009, **113**, 17278.

